Surface-Enhanced Raman Scattering of Hydrogen Plasma-Treated Few-Layer $MoTe_2$

Xiao-Xue Jing(景小雪)[1], Da-Qing Li(李大庆)[2], Yong Zhang(张勇)[1], Xiang-Yu Hou(侯翔宇)[1], Jie Jiang(蒋杰)[1], Xing-Ce Fan(范兴策)[1], Meng-Chen Wang(王梦晨)[1], Shao-Peng Feng(冯少朋)[1], Yuan-fang Yu(于远方), Jun-Peng Lu(吕俊鹏)[1], Zhen-Liang Hu(胡振良)[1*], and Zhen-Hua Ni(倪振华)[1*]

[1]*Department of Physics, Southeast University, Nanjing 211189, China*
[2]*Department of Electronic Engineering, Jiangnan University, Wuxi 214122, China*

(Received 9 April 2021; accepted 14 May 2021; published online 3 July 2021)

Two-dimensional surface-enhanced Raman scattering (SERS) substrates have drawn intense attention due to their excellent spectral reproducibility, high uniformity and perfect anti-interference ability. However, the inferior detection sensitivity and low enhancement have limited the practical application of two-dimensional SERS substrates. To address this issue, we propose that the interaction between the $MoTe_2$ substrate and the analyte rhodamine 6G molecules could be remarkably enhanced by the introduced p-doping effect and lattice distortion of $MoTe_2$ via hydrogen plasma treatment. After the treatment, the SERS is greatly improved, the enhancement factor of probe molecules reaches 1.83×10^6 as well as the limit of detection concentration reaches 10^{-13} M. This method is anticipated to afford new enhancement probability for other 2D materials, even non-metal oxide semiconductor SERS substrates.

DOI: 10.1088/0256-307X/38/7/074203

As an efficient and multi-functional technology for molecular detection, surface-enhanced Raman scattering (SERS) has been broadly used in catalysis chemistry,[1,2] environmental detection,[3,4] and the biological/medical sensing field.[5] The enhancement mechanism can be attributed to two well-known theories: electromagnetic mechanism (EM) and chemical mechanism (CM).[6] Compared with the EM, which derives from the local electromagnetic field generated by the surface plasmon resonance, the CM is concerned with the charge transfer between the substrate and the dye molecules. Some traditional noble material (Au,[7–9] Ag,[10,11] Cu[12]) substrates based on EM have obtained a remarkable SERS effect, however, the extensive applications of these materials are extremely limited by their cost, chemical stability, biocompatibility and surface uniformity. In past decades, 2D material substrates based on CMs, e.g., graphene,[13,14] h-BN[14] and MoS_2,[15] have been proved to be potential candidates for SERS substrates. In addition, they are much more stable, biocompatible and uniform compared to traditional noble metals. Nevertheless, the SERS efficiency of 2D materials is inferior because 2D material SERS substrates are based on a chemical mechanism. According to previous reports, the chemical mechanism enhancement factor is in the range of 10^1–10^2 times,[6] far less than the electromagnetic mechanism (10^6). As a result, one of the most critical challenges now is to explore effective methods to optimize the SERS effect of two-dimensional layered materials.

Numerous methods have been employed in 2D materials to improve the SERS effect, such as doping,[16,17] phase transition[18] and heterostructure formation.[19–21] Among them, chemical doping is a common and efficient method applied to create defects in 2D materials and alter the lattice constants and electronic band structure. Appropriate and reasonable doping can enhance the charge transfer between 2D materials and foreign molecules,[22] thus improving the SERS performance of two-dimensional materials. According to previous reports, doping can be induced in 2D materials by adjusting the CVD synthesis process,[23] electron beam irradiation,[24,25] laser burning,[26] and UV ozone irradiation.[27] However, these techniques have inevitable shortcomings. For instance, laser burning is limited by the low processing area and non-uniform surface of materials after treatment. Electron irradiation and UV ozone irradiation could effectively create defects in a large area, but it is difficult to control the doping degree precisely. The soft plasma technique, a flexible and controllable modification method for materials, has been used to create defect/sites,[28] induce phase transition,[29] and controllably thin of 2D materials.[30] Sun *et al.*[31] have demonstrated that plasma treatment could im-

Supported by the National Natural Science Foundation of China (Grant Nos. 91963130, 11704068, 61927808, and 61705106), the National Key R&D Program of China (Grant No. 2019YFA0308000), the Fundamental Research Funds for the Central Universities (Grant Nos. 2242021k10009, 2242021R20037, and 2242021R20035), and the China Postdoctoral Science Foundation (Grant No. 2018M632197).
*Corresponding authors. Email: phyhzl@seu.edu.cn; zhni@seu.edu.cn
© 2021 Chinese Physical Society and IOP Publishing Ltd

prove the SERS effect of MoS_2, which is attributed to p-doping effect-induced charge transfer enhancement between $MoTe_2$ and probe molecules. Moreover, it has been proved that plasma could modify the intrinsic characteristics of 2D substrates, such as crystal structure[32] and stoichiometry,[33] which contribute to better SERS performance.

In this work, 2H-$MoTe_2$ flakes treated by soft hydrogen plasma present superior SERS effects with a remarkable limit of detection (LOD) as well as enhancement factor (EF). The LOD of rhodamine 6G (R6G) even reaches 10^{-13} M and the corresponding EF is as high as 1.83×10^6. Tellurium vacancies are generated by hydrogen plasma treatment and subsequently react with the ambient oxygen to produce Mo–O bonds, which result in p-type doping. The significant enhancement of $MoTe_2$ SERS substrates is related to the band-filling effect caused by p-type doping, which makes the top of the Mo valence band full of holes and improves the charge transfer between R6G molecules and $MoTe_2$ substrates. Oxygen molecules absorbed on the tellurium vacancies destroy the symmetry of the original $MoTe_2$ lattice and result in distortions of the lattice structure. Raman and x-ray photoelectron spectroscopy (XPS) demonstrate that lattice distortion of hydrogen plasma treated $MoTe_2$ and the introduction of p-doping have led to a significant SERS enhancement. The method of introducing p-doping and generating lattice distortion by plasma may be applicable to other 2D materials, even non-metal oxide semiconductor SERS substrates.

Few-layer 2H-$MoTe_2$ samples are prepared by mechanical exfoliation and transferred on 300 nm SiO_2/Si substrates. The Raman spectra of pristine and hydrogen plasma-treated $MoTe_2$ (H_2-$MoTe_2$) films are displayed in Fig. 1(a). It shows that the pristine $MoTe_2$ films have three Raman vibration modes: in-plane E^1_{2g} mode at $\sim$235 cm^{-1}, out-of-plane A_g mode at $\sim$174 cm^{-1}, and interlayer B_{2g} mode at $\sim$290 cm^{-1}, respectively. Three Raman vibration modes indicate that the sample is in 2H phase. The Raman intensity ratio of B_{2g}/E^1_{2g} of the pristine sample is 0.29, indicating that the $MoTe_2$ flake has three layers.[34] After hydrogen plasma process, the E^1_{2g} and A_g peaks become broader and weaker. It can be ascribed to the defects in the materials induced by hydrogen plasma treatment.[35] On the other hand, vanishing of the B_{2g} peak could be related to the weaker interlayer interaction that was induced by the distortion of $MoTe_2$ lattice.[36] The optical images of H_2-$MoTe_2$ and pristine $MoTe_2$ are displayed in the illustration of Fig. 1(a) and Fig. S1, respectively. The optical image shows that the hydrogen plasma treated sample is identical to the pristine one, which demonstrates that this processing technique is relatively mild. Schematic illustration of the 2D $MoTe_2$ materials treated by hydrogen plasma is shown in Fig. 1(b). During the treatment of the $MoTe_2$ surface, Te atoms overcome the binding force of Mo–Te bonds and produce the tellurium vacancies. The corresponding atomic force microscope (AFM) images are displayed in Figs. 1(c)–1(d). According to the analysis, the thickness of the pristine $MoTe_2$ is 2.6 nm, which can be considered as three layers as well, while the thickness increases to 3.0 nm after plasma treatment. Normally, oxygen molecules in air would not absorb on the $MoTe_2$ surface due to their weak physisorption. However, the stronger interaction between the tellurium vacancy and oxygen molecules promotes the quasi-chemisorption or chemisorption of oxygen molecules at the site of the vacancies.[35,37] Therefore, the increase of the layer thickness is related to the adsorption of oxygen molecules on tellurium vacancies, which is further demonstrated by XPS characterizations.

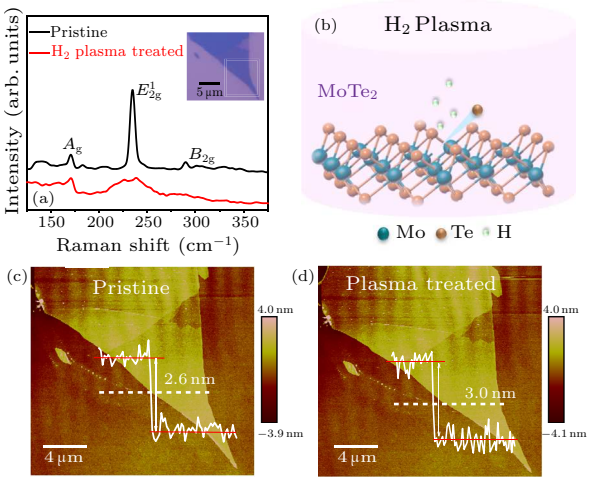

Fig. 1. (a) Raman spectra of the 3L pristine $MoTe_2$ sample and H_2-$MoTe_2$ sample. The inset is the optical images of trilayer $MoTe_2$ flake. (b) Schematic illustration of the 2D $MoTe_2$ materials treated by hydrogen plasma. (c) and (d) AFM images of the pristine $MoTe_2$ and H_2-$MoTe_2$ films, respectively. Height profiles of $MoTe_2$ flakes are indicated in the images.

To explore the change of the atomic concentrations of H_2-$MoTe_2$, XPS spectra of Mo, Te and O are explored, as displayed in Fig. 2. Figure 2(a) reveals that the Mo 3d peak from the original sample can be fitted by two peaks: Mo $3d_{3/2}$ peak at $\sim$230.9 eV and Mo $3d_{5/2}$ peak at $\sim$227.8 eV, suggesting that the Mo atoms in original samples mainly exist at the +4-oxidation state.[38] After hydrogen plasma treatment, new doublet peaks at $\sim$232.5 eV and $\sim$235.3 eV appear, indicating the existence of a +6-oxidation state of Mo.[38] As displayed in Fig. 2(b), the Te 3d spectra have doublet peaks of the Te $3d_{5/2}$ peak at $\sim$572.4 eV and a Te $3d_{3/2}$ peak at $\sim$582.8 eV, resulting from the Mo–Te bonds in $MoTe_2$. New peaks at $\sim$586.3 eV and $\sim$576 eV appear after hydrogen plasma treatment, which are related to the +4-oxidation state of Te.[38] More importantly, the peaks deriving from Mo 3d of

$MoTe_2$ have a red shift by 0.2 eV after plasma treatment compared to the pristine one, indicating the p-type doping of hydrogen plasma.[38,39] Te 3*d* XPS spectra prove the peak position movement as well. Moreover, the Te/Mo ratio extracted from the integral peak area of XPS spectra decreases from ∼2.01 to ∼1.89 after hydrogen plasma treatment, indicating the introduction of Te vacancies. Figure 2(c) shows the O 1*s* spectra of pristine $MoTe_2$ as well as H_2-$MoTe_2$ samples. The O 1*s* spectra from original $MoTe_2$ has one peak at ∼532.2 eV, which is ascribed to the absorbed H_2O on the substrate.[40] After hydrogen plasma treatment, a new peak at ∼530.1 eV appears, indicating the existence of Mo–O bonds.[40] Due to the strong electronegativity of oxygen atoms, the p-doing effect in H_2-$MoTe_2$ is assigned to the oxygen adhesion on the Te vacancy site. The production of the oxidation state of Mo and Te can be explained by the following process: high energy charged particles bombard the $MoTe_2$ surface during hydrogen plasma treatment, Te atoms overcome the binding force of Mo–Te bonds and produce the Te vacancies, then the appearance of tellurium vacancies promotes the absorption of oxygen molecules at the vacancy sites. Once the plasma treated $MoTe_2$ is taken out of the vacuum cavity, it quickly reacts with the oxygen in the air and oxygen molecules adsorb on the $MoTe_2$ substrate. The way that O_2 interacts with H_2-$MoTe_2$ is that one oxygen atom interacts with the two adjacent Te atoms, and the other oxygen atom is attached to the vacancy.[35] In addition, the adsorption of oxygen molecules destroys the symmetry of the original $MoTe_2$ lattice and generate lattice distortions. XPS characterization demonstrates the existence of the Te vacancies and the distortion of the $MoTe_2$ lattice, in consistency with the Raman measurements.

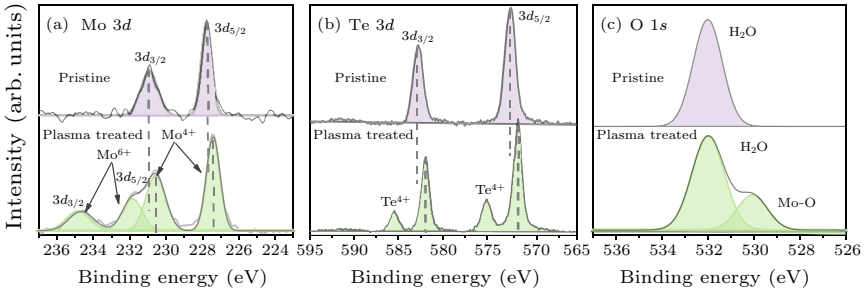

Fig. 2. XPS data obtained from pristine $MoTe_2$ flakes and H_2-$MoTe_2$ flakes. (a) Mo 3*d* peak, (b) Te 3*d* peak and (c) O 1*s* peak from pristine $MoTe_2$ flakes and H_2-$MoTe_2$ flakes, respectively.

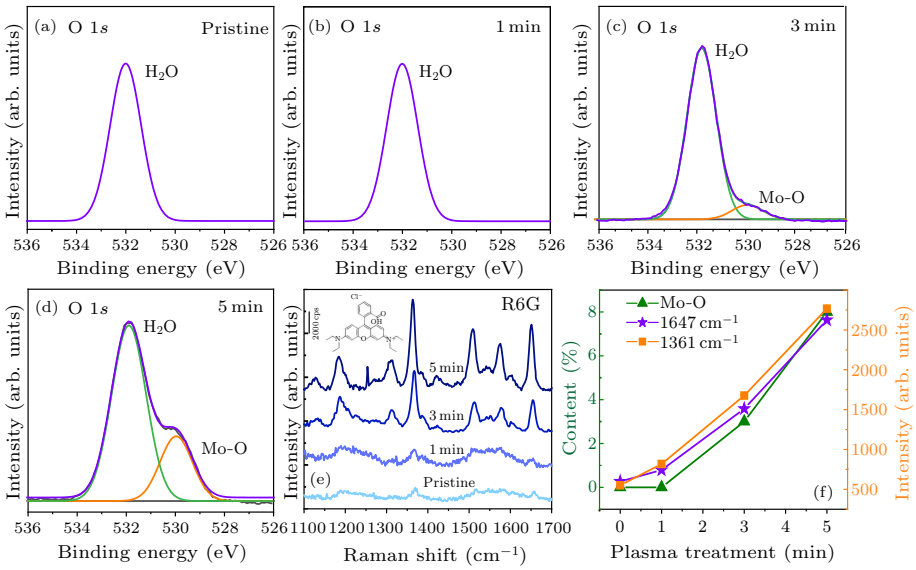

Fig. 3. (a)–(d) The O 1*s* spectra of pristine $MoTe_2$ and those treated with plasma for 1, 3, 5 min. (e) Raman spectra of R6G on $MoTe_2$ and those treated with plasma for different times. (f) The relationship between Raman intensity of the R6G molecule as well as the concentration of the Mo–O peak with plasma treatment time.

The influence of p-doping on H_2-$MoTe_2$ SERS substrates is explored subsequently. Figures 3(a)–3(d) display the XPS spectra of $MoTe_2$ samples with different plasma treatment times (1, 3, and 5 min). The Mo–O peak (∼530.1 eV) appears with an exposure time of 3 min, and the peak intensity of the Mo–O increases with the exposure time. A typical dye molecule rhodamine 6G (R6G) is adopted to inves-

tigate the SERS effect of hydrogen plasma-treated $MoTe_2$ samples. The samples are soaked in the solution of R6G (10^{-7} M) for 40 min, and then rinsed by ethanol. The van der Waals force between R6G molecule and $MoTe_2$ makes R6G physically adsorb on the $MoTe_2$ substrate. The R6G molecule structure (inset) as well as its Raman spectra under various plasma processing times is shown in Fig. 3(e). Raman intensities of R6G increase with the plasma treatment time, in other words, the SERS effect increases with the increasing concentrations of Mo–O in $MoTe_2$. The atomic percentages of oxygen atoms contributed from Mo–O bonds are also calculated in quantitative comparison of the SERS degree of above four samples. Figure 3(f) summarizes the intensities of characteristic Raman modes of R6G molecules (~1361 cm^{-1} and ~1647 cm^{-1}) on the H_2-$MoTe_2$ SERS substrates and the atomic percentage of Mo–O bonds (green curve) as a function of plasma treating time. Firstly, no Mo–O peak content variation is observed, while it increases significantly after 1 min plasma treatment (the content of Mo–O peak is calculated by the ratio of integral peak area of Mo–O peak to the average integral peak area of all ~532.2 peak). Similarly, the Raman intensity of ~1361 cm^{-1} and ~1647 cm^{-1} increases quickly after 1 min treatment. As displayed in Fig. 3(f), Raman intensities as well as Mo–O bonds exhibit the same rising trend with the increasing plasma treatment time. This indicates that the p-doping effect caused by oxygen adsorption on the surface of the $MoTe_2$ substrate has a significant effect on the SERS performance.

Table 1. Comparison of the SERS performances among various non-metal materials.

SERS material	Analyte	LOD(M)	EF	Laser line (nm)	Reference
Graphene	R6G	8×10^{-9}	Unavailable	514	14
n-doped graphene	RhB	1×10^{-11}	Unavailable	514	17
Partially oxidized MoS_2	R6G	10^{-7}	1.4×10^5	532	43
1T′-$MoTe_2$	R6G	4×10^{-13}	1.6×10^8	532	42
a-ZnO nanocages	4-MBA	10^{-5}	6.62×10^5	633	44
Cu_2O superstructure	R6G	10^{-9}	8×10^5	647	45
$W_{18}O_{49}$ nanowire	R6G	10^{-7}	3.4×10^5	532	46
Plasma treated $MoTe_2$	R6G	10^{-13}	1.83×10^6	532	This work

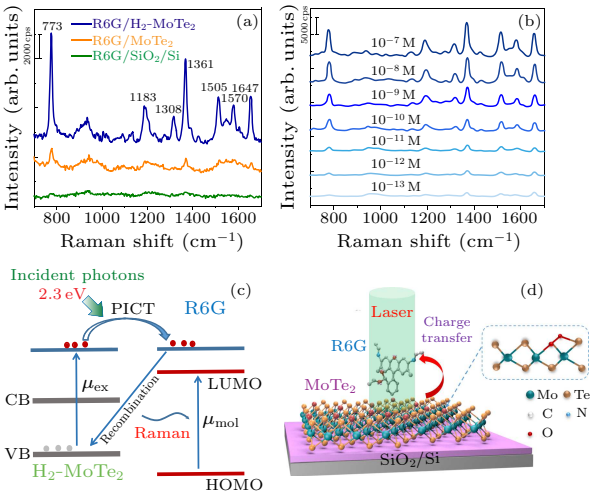

Fig. 4. (a) The comparison of Raman spectra of R6G (10^{-7} M) coated on H_2-$MoTe_2$ and $MoTe_2$ and SiO_2/Si substrates. (b) Raman spectra of R6G deposited on H_2-$MoTe_2$ flakes (3 L) with concentrations ranging from 10^{-7} to 10^{-13} M. (c) Schematic illustration of the charge transfer process in the R6G molecules with the H_2-$MoTe_2$ substrate. (d) Schematic illustration of the 2D $MoTe_2$ as platforms for Raman enhancing of analytes.

Then, the EF and LOD of H_2-$MoTe_2$ are explored to quantitatively determine the enhancement effect. Raman spectra of R6G molecules on the SiO_2/Si substrate, pristine and hydrogen plasma-treated $MoTe_2$ flakes are given in Fig. 4(a). The background noise is subtracted for better comparison. In Fig. 4(a), several Raman peaks of R6G molecules (10^{-7} M) are labeled by ~773, 1183, 1308, 1361, 1505, 1570 and 1647 cm^{-1}. The Raman intensity of R6G on pristine $MoTe_2$ are weak as compared to the plasma-treated one. The Raman characteristic peak of R6G cannot be detected on the SiO_2/Si substrate. To characterize the interaction between the R6G and $MoTe_2$ flake, the Raman signals of R6G with different concentrations are collected as shown in Fig. 4(b). The spectra remain the same except that the Raman peak intensities increase as the concentration increases. It indicates that the R6G molecules do not strongly interact with the substrates, otherwise shifts of the R6G fingerprint peaks would appear.[41] The molecules could be well preserved by the non-destructive property of 2D semiconductor substrates, which is particularly important in molecular recognition and certainly an advantage for SERS substrates. In addition, Raman signatures originating from R6G molecules can also be perceived at the concentration of 10^{-13} M. In comparison to the original $MoTe_2$ substrate with LOD of 10^{-7} M (Fig. S2a) as well as other semiconductor substrates (Table 1),[42–45] the ultra-low LOD of H_2-$MoTe_2$ makes it an ultrasensitive SERS platform.

To quantitatively evaluate the SERS performance of H_2-$MoTe_2$ substrates, EF is calculated according to the molecules Raman strength on the plasma-treated substrate compared with the bare SiO_2/Si substrate. It is noted that an ultrahigh Raman EF (1.83×10^6) is reached for 1647 cm^{-1} (the calculation process is given in the Supporting Information). Further investigation demonstrates that the strong SERS effect could also

be preserved by other probe molecules, such as rhodamine B (RhB). The Raman signals of RhB are distinguishable at low concentration (10^{-11} M), proving the ultrahigh SERS effect of the H_2-$MoTe_2$ for different probes (Fig. S3). The other plasmas as Ar (O_2) are also used to treat $MoTe_2$ samples to explore the Ar (O_2)-$MoTe_2$ substrate SERS effect, as displayed in Fig. S4. SERS effect of Ar (O_2) plasma-treated $MoTe_2$ substrates are the same as hydrogen plasma-treated substrates. It shows that the H_2 (Ar, O_2) plasmas have the same enhancement effect on $MoTe_2$ SERS substrates.

According to the previous reports, the SERS effect of $MoTe_2$ substrates can be ascribed to the photon-induced charge-transfer resonance (PICT).[41] In general, PICT does not emphasize the chemical interaction between the surface and the dye molecules. Instead, it mainly depends on the energy difference between the excited level of the semiconductor and the affinity level of the adsorbed molecule. For the 2D semiconductor, the photon-induced charge-transfer resonance process between the semiconductor substrate and the molecule can be described by a three-step process. First, electrons in the semiconductor valence band (VB) are excited to the excited level as well as holes being created in the VB. Then, the electrons in the excited level absorb the incident photons energy and transfer to the affinity level of the probe molecule. After a short relaxation time, the electrons return to the VB. Currently, electrons keep in an excited state. Finally, the excited electrons recombine with the holes in the VB and emits a Raman photon. Figure 4(c) gives the schematic illustration of the charge transfer process between R6G molecules and the $MoTe_2$ substrate. The highest occupied molecular orbital (HOMO) and the lowest unoccupied molecular orbital (LUMO) levels of R6G molecules are situated at -5.7 and -3.4 eV, and the conduction band (CB) and VB levels of $MoTe_2$ are situated at -3.91 and -4.99 eV, respectively.[13,46] The VB of $MoTe_2$ is much lower than the affinity level of R6G, therefore the PICT process between the $MoTe_2$ substrates and R6G molecule could occur. In addition, the electron transition from HOMO levels to LUMO levels of R6G molecules ($\mu_{\rm mol} \approx 2.3$ eV) can resonate with incident photons, which also enhance the charge transfer. Hence, it can be concluded that exciton resonance ($\mu_{\rm ex}$) of H_2-$MoTe_2$, molecule resonance ($\mu_{\rm mol}$) of R6G as well as the photon-induced charge transfer resonance (PICT) all contribute to the Raman enhancement in the H_2-$MoTe_2$/R6G system. Raman and XPS results confirmed that oxygen absorption at the vacancy site after plasma treatment could induce p-doping and lattice distortion in $MoTe_2$. The VB of $MoTe_2$ has numerous holes after plasma treatment. It accelerates the recombination of the excited electrons transferred from the affinity level of R6G and holes in the VB, and thus promotes the charge transfer process and strengthen the SERS effect of $MoTe_2$ substrates. Furthermore, the distortion of the $MoTe_2$ lattice would weaken the surface potential according to previous reports.[43] More electrons would be transferred from the $MoTe_2$ surface to the probe molecules, and eventually improve the SERS signal. Figure 4(d) shows the schematic illustration of H_2-$MoTe_2$ films as SERS platforms. The SERS effect of R6G molecules on the plasma-treated $MoTe_2$ substrate is attributed to the charge transfer between them.

In summary, we have proved that the hydrogen plasma treatment can remarkably increase the SERS performance of 2D $MoTe_2$ substrates. The detection limit concentration of probe molecules on H_2-$MoTe_2$ can reach the femtomolar level of 10^{-13} M, and the Raman EF can reach 1.83×10^6, which is far beyond previously reported SERS materials such as graphene and non-metal oxide semiconductor substrates. The SERS effect is monotonously enhanced with the increased plasma treatment time. More importantly, our results indicate that the method of generating defects by hydrogen plasma treatment could be expanded to other 2D semiconductor materials, even non-metal oxide semiconductor SERS substrates, which paves the way for the widespread application of semiconductor-based SERS substrates in various fields.

References

[1] Lee D, Choe Y J, Lee M, Jeong D H and Paik S R 2011 *Langmuir* **27** 12782
[2] Ryu H J, Shin H, Oh S, Joo J H, Choi Y and Lee J S 2020 *ACS Appl. Mater. Interfaces* **12** 2842
[3] Alvarez-Puebla R A, dos Santos, Jr David S and Aroca R F 2007 *Analyst* **132** 1210
[4] Pearson B, Mills A, Tucker M, Gao S, McLandsborough L and He L 2018 *Food Microbiol.* **72** 89
[5] Kneipp J, Kneipp H and Kneipp K 2008 *Chem. Soc. Rev.* **37** 1052
[6] Wang X, Shi W, She G and Mu L 2012 *Phys. Chem. Chem. Phys.* **14** 5891
[7] Philip D, Gopchandran K G, Unni C and Nissamudeen K M 2008 *Spectrochim. Acta A: Mol. Biomol. Spectrosc.* **70** 780
[8] Zhang A Q, Wang Q L, Gao Y, Cheng S H and Li H D 2020 *Chin. Phys. Lett.* **37** 068102
[9] Ye X, Shen J, Tao X, Ye G and Yang B 2021 *Chin. Phys. Lett.* **38** 038102
[10] Zhu C, Meng G, Huang Q, Zhang Z, Xu Q, Liu G, Huang Z and Chu Z 2011 *Chem. Commun.* **47** 2709
[11] Zhong Y T, Cheng Z Q, Ma L, Wang J H, Hao Z H and Wang Q Q 2014 *Chin. Phys. Lett.* **31** 047302
[12] Bozzini B, Mele C, D'Urzo L and Romanello V 2006 *J. Appl. Electrochem.* **36** 973
[13] Ling X, Xie L, Fang Y, Xu H, Zhang H, Kong J, Dresselhaus M S, Zhang J and Liu Z 2010 *Nano Lett.* **10** 553
[14] Ling X, Fang W, Lee Y H, Araujo P T, Zhang X, Rodriguez-Nieva J F, Lin Y, Zhang J, Kong J and Dresselhaus M S 2014 *Nano Lett.* **14** 3033
[15] Muehlethaler C, Considine C R, Menon V, Lin W C, Lee

Y H and Lombardi J R 2016 *ACS Photon.* **3** 1164
[16] Zhang R, Drysdale D, Koutsos V and Cheung R J 2017 *Adv. Funct. Mater.* **27** 1702455
[17] Feng S, Dos S M C, Carvalho B R, Lv R, Li Q, Fujisawa K, Elias A L, Lei Y, Perea-Lopez N and Endo M J 2016 *Sci. Adv.* **2** e1600322
[18] Ying Y, Peng M, Zhang Y M, Han J C, Zhang X H *et al.* 2017 *Adv. Funct. Mater.* **27** 1606694
[19] Wang P, Xia M, Liang O, Sun K, Cipriano A F, Schroeder T, Liu H and Xie Y H 2015 *Anal. Chem.* **87** 10255
[20] Tan Y, Ma L, Gao Z, Chen M and Chen F 2017 *Nano. Lett.* **17** 2621
[21] Zhang L S, Fang Y and Wang P J 2012 *Chin. Phys. Lett.* **29** 114210
[22] Yao J, Quan Y, Gao R, Li J, Chen L, Liu Y, Lang J, Shen H, Wang Y, Yang J and Gao M 2019 *Langmuir* **35** 8921
[23] Zhou W, Zou X, Najmaei S, Liu Z, Shi Y, Kong J, Lou J, Ajayan P M, Yakobson B I and Idrobo J C 2013 *Nano Lett.* **13** 2615
[24] Leiter R, Li Y and Kaiser U 2020 *Nanotechnology* **31** 495704
[25] Komsa H P, Kotakoski J, Kurasch S, Lehtinen O, Kaiser U and Krasheninnikov A V 2012 *Phys. Rev. Lett.* **109** 035503
[26] Chen J, Zhu J, Wang Q, Wan J and Liu R 2020 *Small* **16** 2001428
[27] Tomašević-Ilić T, Jovanović Đ, Popov I, Fandan R, Pedrós J, Spasenović M and Gajić R 2018 *Appl. Surf. Sci.* **458** 446
[28] Kong X, Xu Y, Cui Z, Li Z, Liang Y, Gao Z, Zhu S and Yang X 2018 *Appl. Catal. B: Environ.* **230** 11
[29] Zhu J, Wang Z, Yu H, Li N, Zhang J, Meng J, Liao M, Zhao J, Lu X, Du L, Yang R, Shi D, Jiang Y and Zhang G 2017 *J. Am. Chem. Soc.* **139** 10216
[30] Zhang L, Feng S, Xiao S, Shen G, Zhang X, Nan H, Gu X and Ostrikov K 2018 *Appl. Surf. Sci.* **441** 639
[31] Sun L, Hu H, Zhan D, Yan J, Liu L, Teguh J S, Yeow E K, Lee P S and Shen Z 2014 *Small* **10** 1090
[32] Ouyang B, Zhang Y, Xia X, Rawat R S and Fan H J 2018 *Mater. Today Nano* **3** 28
[33] Ctibor P, Štengl V, Píš I, Zahoranová T and Nehasil V 2012 *Ceram. Int.* **38** 3453
[34] Ruppert C, Aslan O B and Heinz T F 2014 *Nano Lett.* **14** 6231
[35] Chen B, Sahin H, Suslu A, Ding L, Bertoni M I, Peeters F M and Tongay S 2015 *ACS. Nano.* **9** 5326
[36] Islam M R, Kang N, Bhanu U, Paudel H P, Erementchouk M, Tetard L, Leuenberger M N and Khondaker S I 2014 *Nanoscale* **6** 10033
[37] Liu H, Han N and Zhao J 2015 *RSC Adv.* **5** 17572
[38] Zheng X, Wei Y, Deng C, Huang H, Yu Y, Wang G, Peng G, Zhu Z, Zhang Y, Jiang T, Qin S, Zhang R and Zhang X 2018 *ACS Appl. Mater. Interfaces* **10** 30045
[39] Qu D, Liu X, Huang M, Lee C, Ahmed F, Kim H, Ruoff R S, Hone J and Yoo W J 2017 *Adv. Mater.* **29** 1606433
[40] Zuo P, Jiang L, Li X, Ran P, Li B, Song A, Tian M, Ma T, Guo B, Qu L and Lu Y 2019 *Nanoscale* **11** 485
[41] Tao L, Chen K, Chen Z, Cong C, Qiu C, Chen J, Wang X, Chen H, Yu T, Xie W, Deng S and Xu J B 2018 *J. Am. Chem. Soc.* **140** 8696
[42] Zheng Z, Cong S, Gong W, Xuan J, Li G, Lu W, Geng F and Zhao Z 2017 *Nat. Commun.* **8** 1993
[43] Wang X, Shi W, Jin Z, Huang W, Lin J, Ma G, Li S and Guo L 2017 *Angew. Chem. Int. Ed. Engl.* **56** 9851
[44] Lin J, Shang Y, Li X, Yu J, Wang X and Guo L 2017 *Adv. Mater.* **29** 1604797
[45] Cong S, Yuan Y, Chen Z, Hou J, Yang M, Su Y, Zhang Y, Li L, Li Q, Geng F and Zhao Z 2015 *Nat. Commun.* **6** 7800
[46] Li C, Yan X, Song X, Bao W, Ding S, Zhang D W and Zhou P 2017 *Nanotechnology* **28** 415201

Supporting Information for "Surface-Enhanced Raman Scattering of Hydrogen Plasma-Treated Few-Layer $MoTe_2$"

Xiao-Xue Jing(景小雪)[1], Da-Qing Li(李大庆)[2], Yong Zhang(张勇)[1], Xiang-Yu Hou(侯翔宇)[1], Jie Jiang(蒋杰)[1], Xing-Ce Fan(范兴策)[1], Meng-Chen Wang(王梦晨)[1], Shao-Peng Feng(冯少朋)[1], Yuan-Fang Yu(于远方)[1], Jun-Peng Lu(吕俊鹏)[1], Zhen-Liang Hu(胡振良)[1*], and Zhen-Hua Ni(倪振华)[1*]

[1] *Department of Physics, Southeast University, Nanjing 211189, China.*

[2] *Department of Electronic Engineering, Jiangnan University, Wuxi 214122, China.*

1. Experimental Methods

Sample Preparation. Few layer $MoTe_2$ films were prepared by mechanical exfoliation method from the bulk $MoTe_2$ crystal, and transferred onto 300 nm SiO_2/Si substrates. Then the samples were treated with hydrogen plasma at 100 w under the pressure of 5 Pa.

Characterization. The Dimension ICON AFM equipment was used to identify the thickness of the original and hydrogen plasma treated $MoTe_2$ (H_2-$MoTe_2$) samples, and the Thermo Fisher XPS equipment was used to detect the atomic concentrations and valence state of the original and H_2-$MoTe_2$ samples. All Raman spectra were collected by the LABRAM HR-800 Raman equipment with the laser line of 532nm.

SERS measurement. The 10^{-7} ~ 10^{-13} M R6G aqueous solution were diluted from 10^{-3} M aqueous solution in the certain proportion. The prepared samples were soaked in a specific solution for 40 minutes (The samples were soaked in the solution for enough time to ensure that the concentration of the R6G/RhB molecules on $MoTe_2$ sample is the same as in the solution), then taken out and rinse with ethanol, and finally blown with nitrogen. Raman spectrum were collected with a 50 × L objective lens; the laser spot diameter was about 1 μm; the laser power was 0.5 mW and the acquisition time was 40 s. Raman spectra were measured at 15 different locations on each sample, and the mean value of signal intensity was taken as the standard deviation for the final analysis standard.

2. Optical microscopy images of pristine and H_2-$MoTe_2$ film

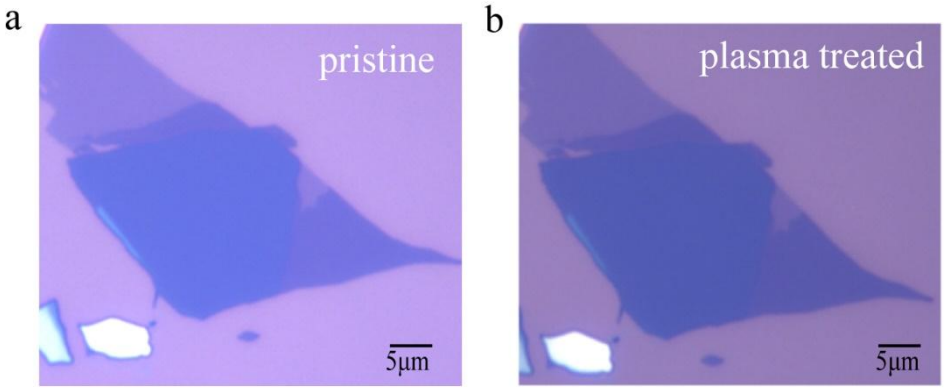

Fig. S1. Optical microscopy images of pristine and hydrogen plasma treated $MoTe_2$ films on 300-nm SiO_2/Si substrates.

3. Raman spectra of R6G molecules coated on pristine $MoTe_2$ and H_2-$MoTe_2$ substrates

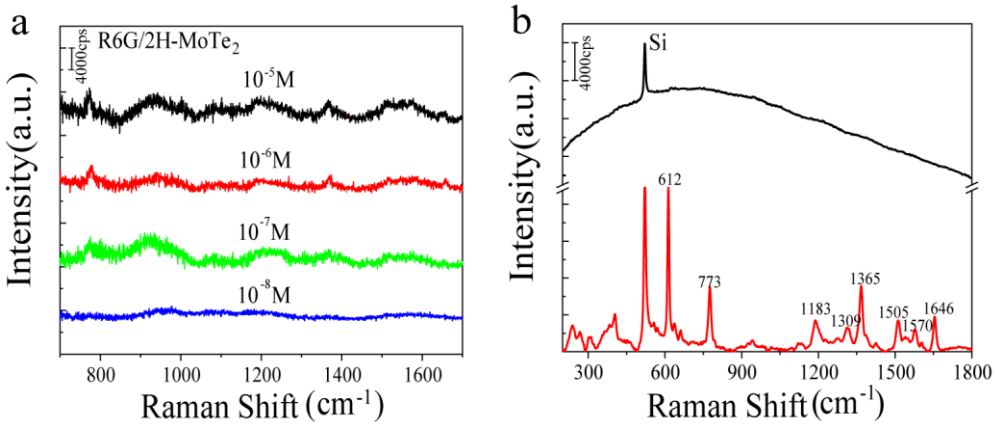

Fig. S2. (a) SERS spectra of R6G coated on pristine $MoTe_2$ flakes (3L) with various concentrations from 10^{-5} to 10^{-8} M. (b) Raman spectra of the R6G molecules deposited on bare SiO_2 (black line) and on 2D H_2-$MoTe_2$ (red line). The signal integration times were both 40 s.

4. The calculated enhancement factors

The Raman enhancement factors (EF) of the substrates were estimated according to the following equation (1)[1, 2]

$$E_{\mathrm{f}} = \frac{I_{SERS}/N_{SERS}}{I_{bulk}/N_{bulk}} \qquad (1)$$

where I_{SERS} and I_{bulk} represent the Raman intensity of probe molecules on hydrogen plasma treated $MoTe_2$ substrate and the Raman intensity measured from the bulk probe molecules without substrate, respectively. N_{SERS} and N_{Bulk} denote the corresponding numbers of probe molecules on H_2 plasma treated $MoTe_2$ substrate and that without substrate, respectively. N_{SERS} is written as $N_{SERS} = \frac{CVN_A A_{Raman}}{A_{sub}}$ and N_{bulk} is written as $N_{bulk} = \frac{\rho h A_{Raman}\ N_A}{M}$. C is the corresponding concentration of probe molecules (10^{-7} M) and V is the volume of the droplet (20 μL), h is the effective layer

depth of 21 μm[3]. N_A is the Avogadro constant and A_{Raman} is the laser spot area. A_{sub} is the effective area of the substrate, which is approximately 9π mm^2. M is the molar mass of dye (479.02 g/mol for R6G) and density ρ of bulk R6G is 1.15 g cm^{-3}.

For the SERS measurement, the intensity is obtained by taking average from measurements of 15 spots, and the number of analyte molecules is estimated by equation (1) on the assumption that the analyte molecules were distributed uniformly on the substrates. The peak of 1647 cm^{-1} was selected to calculate the enhancement factor. The Raman 1647 cm^{-1} intensity of R6G/H_2-$MoTe_2$ (10^{-7} M) is 3940 counts with 40 s acquisition time, and that of bulk R6G is 3700 counts with 1 s acquisition time. From the observed spectra we obtain for the ratio of intensities I_{SERS} / I_{Bulk} = (3940/40)/ (3700/1) =2.7×10^{-2}. The EF at 10^{-7} M dye concentration is estimated to be around 1.83 × 10^6.

5. Raman spectra of RhB molecules on H_2-$MoTe_2$, $MoTe_2$ and SiO_2 substrates

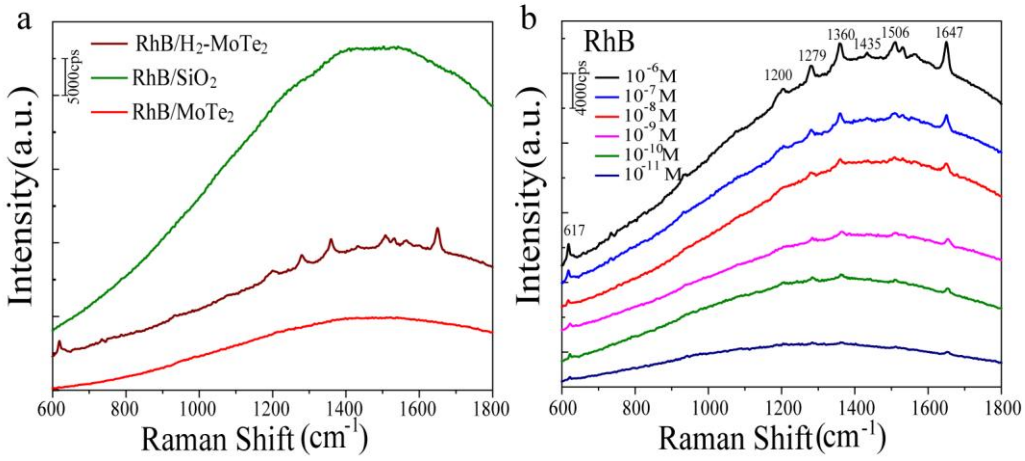

Fig. S3. (a) Raman spectra of RhB coated on H_2-$MoTe_2$, $MoTe_2$ and SiO_2 substrates with a fixed concentration of 10^{-7} M. (b) SERS spectra of RhB coated on H_2-$MoTe_2$ flakes (3L) with various concentrations from 10^{-6} to 10^{-11} M.

6. Raman spectra of R6G molecules on Ar(O_2)-$MoTe_2$ substrates

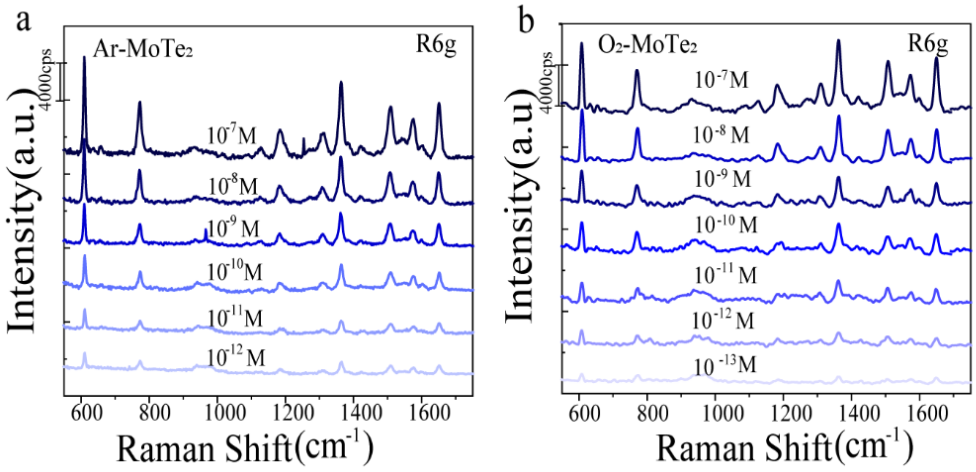

Fig. S4. (a) Raman spectra of R6g coated on Ar-$MoTe_2$ substrates with various concentrations from 10^{-7} to 10^{-12} M. (b) Raman spectra of R6g coated on O_2-$MoTe_2$ substrates with various concentrations from 10^{-7} to 10^{-13} M.

Supplementary references

[1] Chen K, Chen Z, Wan X, Zheng Z, Xie F, Chen W, Gui X, Chen H, Xie W and Xu J 2017 *Advance Materials* **29** 482

[2] Mehmet, Yilmaz, Esra, Babur, Ozdemir, Rebecca L, Gieseking, Yavuz, Dede and Ugur 2017 *Nature materials* **141** 4097

[3] Cai W B, Ren B, Li X Q, She C X, Liu F M, Cai X W and Tian Z Q 1998 *Surface Science* **406** 9